Human-in-the-Loop Bicycle Control via Active Heart Rate Regulation

Matteo Corno, Paolo Giani, Mara Tanelli, and Sergio Matteo Savaresi

I. Introduction

EVER increasing fossil fuel's cost and environmental concerns are promoting the search for more efficient means of transportation. (Hybrid) Electric vehicles are among the options that received most of the attention. There are, however, other, possibly more efficient transportation systems. Bicycles, for example, are extremely cost effective, eco-friendly, and healthy and, in congested cities, are the fastest way to reach one's destination. For these reasons, bicycles have attracted a considerable amount of industrial and academic interests (see [10], [17], [20], [26], and references cited therein).

Although easy to use and efficient, bicycles are not always perceived as a viable commuting option. The cycling commute route may be too long and tiring. Two solutions have been put forward to address this issue. On the one side, municipalities all over the world are promoting the concept of bike sharing [16], [25]. According to this model, the user travels to the city via public means of transportation and then rent as she goes a bicycle to cover the *last mile*.

Another option is that of physically helping the cyclist to cover the mid-distance commute. Electric power assisted cycles (EPACs) [22], [28], [29], [35] implement this solution. EPACs, by providing torque assistance through an electric motor, considerably lower the pedaling physical effort, and are experiencing a huge commercial success. However, added cost of electronics, batteries, and motor is not negligible, so that an EPAC could cost three times a traditional bicycle.

Advances in mechatronic systems are opening a third path, namely intelligent passive bikes. These kinds of bikes do not directly provide assisting traction power, but rather modify the vehicle response to the cyclist's input. An example of such systems is automated gear shifting, implemented through discrete gear shifting or continuously varying transmissions (CVTs) [12].

Intelligent passive bikes have less potential than EPACs of reducing the cyclist's fatigue and physical effort but are considerably simpler and thus may represent an interesting and more accessible alternative. This direction is relatively new and only a handful of contributions are available; among the most interesting ones, one can find [8], [33], and [35]. In [33], the authors design a cost effective automated derailleur/multisprocket system. The control system is designed to keep the pedaling cadence in a comfort zone. Also in [35], the focus is on the mechatronic actuator design. Chien and Tseng [8] implement a learning algorithm that determines the optimal transmission ratio based on the pedaling cadence and pedaling power (estimated through a model).

In this paper, a different approach is taken, in that the transmission ratio of a CVT is modulated with the objective of controlling the cyclist's heart rate (HR). The control system modulates the transmission ratio so to keep the cyclist's HR at a user-specified value. The rationale behind this concept is that the HR is a proxy of fatigue [6], [27]; by keeping the HR constant, one can better distribute her or his physical effort through the cycling trip. This paper is structured in three main parts; modeling, control, and validation. In the modeling part, a control-oriented model of the entire system is derived. The model has two main components, the model of the CVT-equipped bicycle and the model of the HR dynamics. A CVT has been preferred to more common bicycle gear systems (i.e., the derailleur/multisprocket system) for the possibility of continuously modulating the transmission. See [12] for a detailed discussion on the advantages and control issues that arise in applying a CVT to a bicycle. This paper extends the preliminary results of [14] by more thoroughly discussing the model, the control system design, and the experimental results.

Manuscript received November 29, 2013; revised August 10, 2014; accepted September 23, 2014. Date of publication October 16, 2014; date of current version April 14, 2015. Manuscript received in final form September 26, 2014. This work was supported by the Regione Lombardia through the Green Mov Project. Recommended by Associate Editor M. Guay.

The authors are with the Dipartimento di Elettronica, Informazione e Bioingegneria, Politecnico di Milano, Milan 20133, Italy (e-mail: corno@elet.polimi.it; paolo.giani@polimi.it; mara.tanelli@polimi.it; savaresi@elet.polimi.it).

Color versions of one or more of the figures in this paper are available online.

HR dynamic modeling is an extremely rich field in biomechanics literature. The available models can be classified into two main categories, namely the *linearised* and *nonlinear* modeling approaches. In the first class, the system dynamics are expressed as the sum of two or more terms generated by linear systems. According to [5], when the exercise starts, two time constants are in general involved: the first explains the nervous system actions, and a second, slower, one is related to the changes in metabolic activity and to the lactate production. One of the first and most widely accepted models is a second-order linear model [15]. The system linearity is interesting from a control perspective; however, it can be inaccurate if demanding physical exercises are considered. To cope with this issue, time-varying versions of linear models have been recently proposed [19].

Among the nonlinear models, in [7], a physiological-based second-order nonlinear state space model has been proposed to describe the HR dynamics during and after a treadmill exercise. A different dynamical nonlinear model has been derived from physiological time series in [36], where stochastic optimization methods have been adopted to identify the model parameters. The same model has been also investigated in [30] and [37], demonstrating the fitting of the model output to a set of raw data for multiple constant intensity exercises. Finally, the Hammerstein model proposed in [31] seems to be an interesting compromise between the simplicity of linear models and the accuracy of nonlinear ones. The authors show that this modeling approach provides a reliable and effective model, and a satisfactory control performance is achieved [18], [21], [32]. The goal of the HR dynamic modeling part of this paper is not that of providing a complete general model of the HR dynamics but rather get to a control-oriented model valid for moderate cycling efforts, typical of leisure, and commuting cycling. The control-oriented model is the basis to develop the control strategy.

From the control design point of view, no matter how well a model describes the HR response of any given subject, intersubject variability, and exogenous factors (such as ambient temperature and humidity) necessarily generate uncertainties that need to be accounted for. In this paper, two control solutions to deal with this issue are presented: a linear feedback controller and a second-order sliding mode (SOSM) controller. The sliding mode controller guarantees a higher level of robustness and it is thus preferred. The validity of the proposed control system is tested on two subjects on a series of trials designed to mimic real word usage.

This paper is structured as follows. In Section II, the modeling of the overall system is discussed. In Section III, two control systems are designed and tested using step responses. The SOSM controller is finally validated during normal cycling by several subjects in Section IV.

II. System Description and Modeling

The overall control system architecture, shown in Fig. 1, has several components: the bicycle, the cyclist's pedaling dynamics, the cyclist's HR dynamics, and the controller.

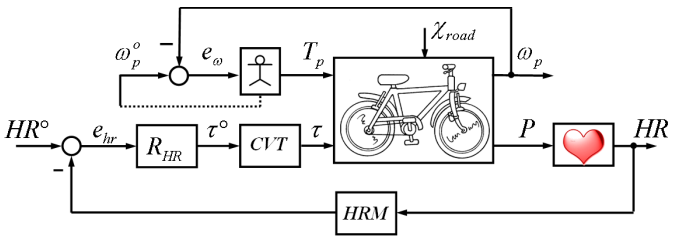

Fig. 1. Overall control system architecture.

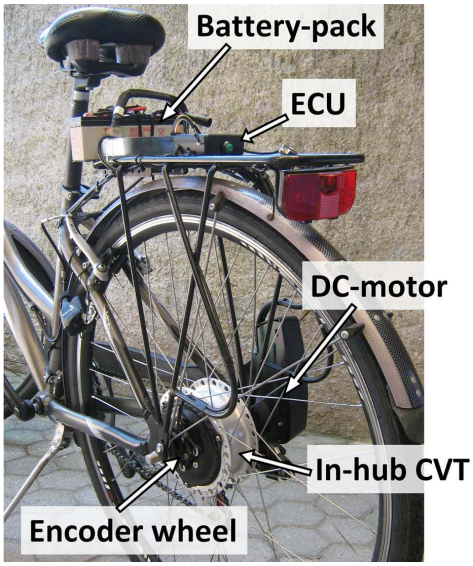

Fig. 2. Instrumented bicycle employed in this paper.

This section analyses and details the bicycle, cyclist, and HR dynamic models.

A. Bicycle

The test vehicle (Fig. 2) is a standard city bike equipped with a NuVinci roller-based CVT with a freewheel [11]. The freewheel transmits only positive torque to the wheel. The CVT comes with power electronics that, by means of a dc motor, modulates the transmission ratio. The desired transmission ratio is set by an additional custom electronic control unit (ECU). The ECU also measures some CVT quantities, such as the dc-motor angular position, and vehicle variables, as pedal speed and rear wheel speed. The bicycle is also equipped with a pedal torque sensor that is only used in analysis but not for control purposes. The experimental layout also includes an Onyx II 9560BT HR Monitor (indicated as HRM in the schematics of Fig. 1) for HR measurement.

The HR control algorithm runs on a Smartphone, while the ECU performs the low-level CVT control. The three devices (HRM, Smartphone, and ECU) communicate via Bluetooth. The vehicle is equipped with a small battery pack (12 V, 2.5 Ah) that supplies both the CVT and the ECU electronics.

From the control point of view, there are two components of interest: the transmission and the road load. The balance of

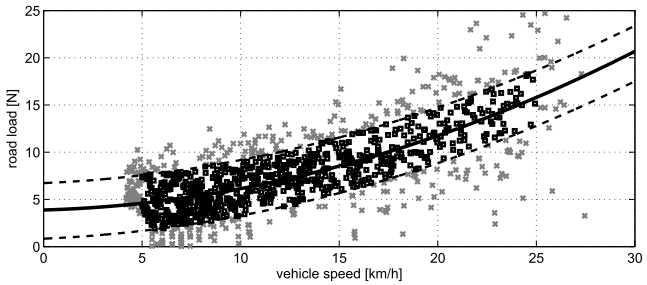

Fig. 3. Identification of the overall friction forces acting on the bicycle.

the forces acting of the bicycle yields the road-load equation

$$M_v\dot{v} = -\frac{1}{2}\rho C_x A v^2 - D_v v + \\ - M_v g(\sin(\mathcal{X}_{\text{road}}) + C_r\cos(\mathcal{X}_{\text{road}})) + F_w \quad (1)$$

where M_v is the bicycle mass and v its longitudinal velocity. The road load is the sum of several contributions.

1) $(\rho C_x A_v^2)/2$ represents the aerodynamic drag: ρ is the air density, A the vehicle front area, and C_x the drag coefficient.
2) $D_v v$ describes the viscous friction effects due to wheel bearings and other mechanical elements.
3) $M_v g\sin(\mathcal{X}_{\text{road}})$ represents the gravitational force, where $\mathcal{X}_{\text{road}}$ is the road slope and g is the acceleration of gravity.
4) $M_v g C_r\cos(\mathcal{X}_{\text{road}})$ models the rolling resistance, depending on the normal force on the tires-road contact surface and on the friction coefficient C_r.
5) F_w is the traction force generated by the wheel.

Note that only the longitudinal dynamics are modeled. The model parameters are either measured (as in the case of the mass) or identified from a so-called coasting down experiment performed on a flat road [1]. The results of the parameter identification procedure are shown in Fig. 3. The figure plots the measured road load in several experiments performed at constant velocity on a flat road and its optimal fitting (along with the confidence intervals). Note the high level of noise affecting the road load; in fact, it depends on the cyclist's posture, wind, and road disturbances.

The transmission is assumed to be rigid, so that the ratio between the vehicle velocity v and the pedaling cadence ω_p is instantaneously determined by the CVT ratio τ according to

$$\tau = \frac{r_w v}{\omega_p} \quad (2)$$

where r_w is the rear wheel rolling radius. The wheel force F_w is the cyclist's pedal torque T_p as transmitted by the bicycle transmission and tire-road friction. Assuming that the tire has negligible slip, the transmission dynamics is given by

$$J\dot{\omega}_p = T_p - D\omega_p - \frac{\tau r_w}{\eta}F_w \quad (3)$$

where η is the transmission efficiency (identified to be 0.87—see [13] for more details on the identification); J and D are the transmission mass moment of inertia and friction factor than can be identified with ad hoc experiments performed on the single components.

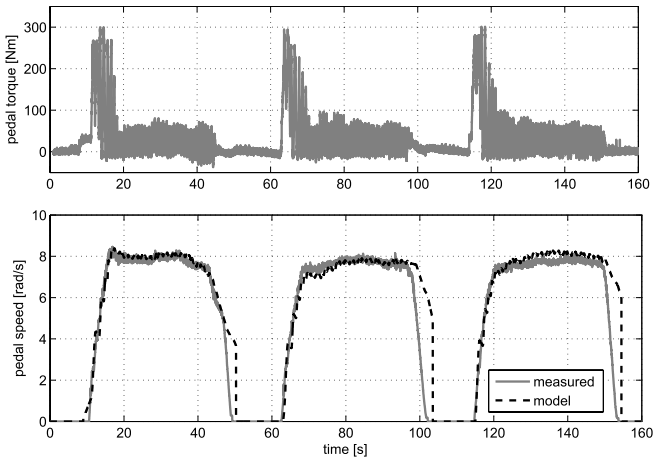

Fig. 4. Results of the validation experiments for the longitudinal dynamic model.

Combining the transmission and the road-load model, one obtains the complete longitudinal model

$$J\dot{\omega}_p = T_p - D\omega_p \\ + \frac{\tau^2 r_w^2}{\eta}\Big(M_v\dot{\omega}_p + \frac{1}{2}\tau r_w\rho C_x A\omega_p^2 + D_v\omega_p\Big) \\ + \frac{\tau r_w}{\eta}(M_v g\sin(\mathcal{X}_{\text{road}}) + M_v g C_r\cos(\mathcal{X}_{\text{road}})). \quad (4)$$

The overall model is validated comparing the simulated velocity with the measured one as a response to measured pedal torque inputs. Fig. 4 shows that the fitting between the two models is satisfactory. Note that in the deceleration phase, the model underestimates the deceleration; the reason is that during the tests the cyclist braked. The friction brakes are not modeled as they do not play a role in the control problem.

Equation (4) describes one of the critical dynamic components of the control problem; as such it deserves an in-depth analysis. It has three inputs: cyclist torque, transmission ratio, and road slope. The role of the inputs is better understood by defining the following parameters:

$$M_v^* = \frac{r_w^2 M_v}{\eta}, \quad \sigma_0^* = \frac{r_w M_v g}{\eta}, \quad \sigma_1^* = \frac{r_w^2 D_v}{\eta} \\ \sigma_2^* = \frac{r_w^3\rho C_x A}{2\eta}, \quad \sigma_3^* = \frac{r_w M_v g C_r}{\eta} = \sigma_0^* C_r. \quad (5)$$

Substituting the above definitions into (4), the system model becomes

$$\dot{\omega}_p = \frac{1}{J + \tau^2 M_v^*}\Big[T_p - \sigma_2^*\tau^3\omega_p^2 - \big(D + \sigma_1^*\tau^2\big)\omega_p \\ + \tau\Lambda\sin\left(\mathcal{X}_{\text{road}} + \phi\right)\Big] \\ = f_\omega(\omega_p, T_p, \tau, \mathcal{X}_{\text{road}}) \quad (6)$$

where the road slope terms are collected in

$$\Lambda\sin(\mathcal{X}_{\text{road}} + \phi) = \sigma_0^*\sin(\mathcal{X}_{\text{road}}) + \sigma_3^*, \cos(\mathcal{X}_{\text{road}}) \quad (7)$$

with $\Lambda = ((\sigma_0^*)^2 + (\sigma_3^*)^2)^{1/2}$ and $\phi = \arctan(\sigma_3^*/\sigma_0^*)$.

Equation (6) is a dynamical first-order nonlinear system with state variable ω_p and three input variables, namely the

pedal torque T_p, the transmission ratio τ, and the road slope $\mathcal{X}_{\text{road}}$. The system response to the input can be analyzed linearizing it. Linearization implies the seeking of equilibria of (6).

For a given triplet $(\overline{T}_p, \overline{\tau}, \overline{\mathcal{X}}_{\text{road}})$, the equilibrium pedal velocity $\bar{\omega}_p$ is

$$\bar{\omega}_p = \frac{\Gamma \pm \sqrt{\Gamma^2 + \Delta}}{-2\sigma_2^* \bar{\tau}^3} \tag{8}$$

where

$$\begin{aligned} \Gamma &= D + \sigma_1^* \bar{\tau}^2 \\ \Delta &= 4\sigma_2^* \bar{\tau}^3 (\bar{T}_p - \bar{\tau} \Lambda \sin(\overline{\mathcal{X}}_{\text{road}} + \phi)). \end{aligned} \tag{9}$$

Not all triplets yield a feasible equilibrium ω_p. Two constraints need to be accounted for: 1) only positive real $\bar{\omega}_p$ are feasible and 2) due to the freewheel, no negative torque can be transmitted from the pedals to the rear wheel, i.e., $\bar{T}_p \geq 0$. These conditions translate into

$$\bar{T}_p \geq \max\{0, \bar{\tau} \Lambda \sin\left(\overline{\mathcal{X}}_{\text{road}} + \phi\right)\}. \tag{10}$$

Hence, for a given combination of constant inputs $(\overline{T}_p, \overline{\tau}, \overline{\mathcal{X}}_{\text{road}})$ satisfying (10), it is possible to compute the corresponding equilibrium value of the pedal speed and derive the linearized model from (6) as

$$\begin{aligned} \delta\dot{\omega}_p = &\left.\frac{\partial f_\omega}{\partial \omega}\right|_{\left(\overline{T}_p, \overline{\tau}, \overline{\mathcal{X}}_{\text{road}}\right)} \delta\omega + \left.\frac{\partial f_\omega}{\partial T_p}\right|_{\left(\overline{T}_p, \overline{\tau}, \overline{\mathcal{X}}_{\text{road}}\right)} \delta T_p \\ &+ \left.\frac{\partial f_\omega}{\partial \tau}\right|_{\left(\overline{T}_p, \overline{\tau}, \overline{\mathcal{X}}_{\text{road}}\right)} \delta\tau + \left.\frac{\partial f_\omega}{\partial \mathcal{X}_{\text{road}}}\right|_{\left(\overline{T}_p, \overline{\tau}, \overline{\mathcal{X}}_{\text{road}}\right)} \delta\mathcal{X}_{\text{road}} \end{aligned} \tag{11}$$

where δ has the usual meaning of a perturbation around the equilibrium. This produces the linearized model equation

$$\delta\dot{\omega}_p = A\delta\omega_p + B_0\delta T_p + B_1\delta\tau + B_2\delta\mathcal{X}_{\text{road}} \tag{12}$$

where

$$\begin{aligned} A &= -\left(D + 2\sigma_2^* \overline{\tau}^3 \overline{\omega}_p + \sigma_1^* \overline{\tau}^2\right)/E \\ B_0 &= \frac{1}{E} \\ B_1 &= -\left(3\sigma_2^* \overline{\tau}^2 \overline{\omega}_p^2 + 2\sigma_1^* \overline{\tau\omega}_p + \Lambda \sin\left(\overline{\mathcal{X}}_{\text{road}} + \phi\right)\right)/E \\ B_2 &= -\overline{\tau}\Lambda \cos(\overline{\mathcal{X}}_{\text{road}} + \phi)/E \\ E &= J + \overline{\tau}^2 M_v^*. \end{aligned} \tag{13}$$

It can be easily shown that all admissible equilibriums are asymptotically stable. Finally, applying the Laplace transformation to (12), three transfer functions can be derived linking the three system inputs to the pedal speed, namely $G_{T\omega}(s)$, $G_{\tau\omega}(s)$, and $G_{\mathcal{X}\omega}(s)$. All these first-order transfer functions share the common time constant

$$T_\omega = \frac{J + \overline{\tau}^2 M_v^*}{D + 2\sigma_2^* \overline{\tau}^3 \overline{\omega}_p + \sigma_1^* \overline{\tau}^2}. \tag{14}$$

Fig. 5 shows the values of T_ω for different equilibrium points. As apparent, the time constant increases as the speed or the transmission ratio decreases.

A brief analysis of the three transfer functions is now provided.

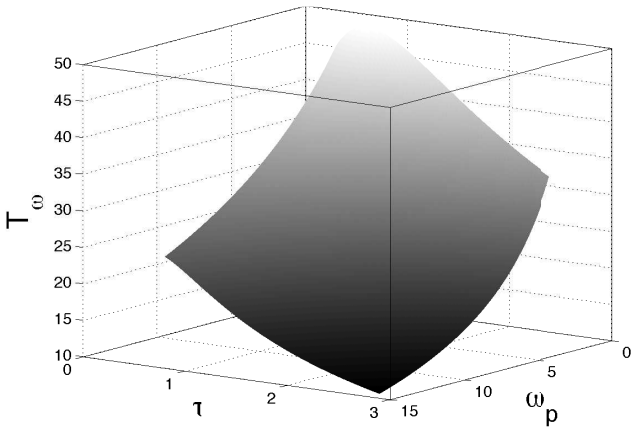

Fig. 5. Time constant T_ω as a function of the equilibrium point.

1) Torque Transfer Function $G_{T\omega}(s)$: The transfer function from pedal torque to pedal cadence is

$$G_{T\omega}(s) = \frac{\mu_T}{sT_\omega + 1} \tag{15}$$

where T_ω is as in (14), and the gain μ_T has the form

$$\mu_T = \frac{1}{D + 2\sigma_2^* \overline{\tau}^3 \overline{\omega}_p + \sigma_1^* \overline{\tau}^2}. \tag{16}$$

The following remarks can be made as follows.

1) The gain is always positive. This is quite intuitive: if the transmission ratio is constant, an increase in torque determines an increase in the pedaling cadence.
2) The gain depends on the transmission ratio: the higher the transmission ratio, the lower the gain (i.e., the less sensitive the pedaling cadence is to the torque variation).
3) The gain depends on the pedaling cadence: the gain decreases as the pedaling cadence decreases. This effect is determined by σ_2, which accounts for the aerodynamic effects.

2) Transmission Ratio Transfer Function $G_{\tau\omega}(s)$: It is a first-order system with time constant T_ω. Its gain is

$$\mu_\tau = -\frac{3\sigma_2^* \bar{\tau}^2 \overline{\omega}_p^2 + 2\sigma_1^* \overline{\tau\omega}_p + \Lambda \sin\left(\overline{\mathcal{X}}_{\text{road}} + \phi\right)}{D + 2\sigma_2^* \overline{\tau}^3 \overline{\omega}_p + \sigma_1^* \overline{\tau}^2}. \tag{17}$$

It can be shown that, for all admissible equilibriums, the gain is negative. This explains the fact that the pedal speed decreases as the transmission ratio increases. The additive term (7), which depends on $\bar{\mathcal{X}}_{\text{road}}$, makes the gain decrease as the road slope increases. Fig. 6 plots μ_τ as a function of transmission ratio and road slope for pedal cadences, namely $\bar{\omega}_p = 4$ rad/s and $\bar{\omega}_p = 16$ rad/s, corresponding to 40 and 150 r/min, respectively (the minimum and the maximum pedal speed reasonably achieved in normal riding conditions). As it can be seen, the gain exhibits significant variations as a function of $\bar{\omega}_p$ if $\bar{\tau} \lesssim 1.5$, and it is highly influenced by $\bar{\mathcal{X}}_{\text{road}}$ and $\bar{\tau}$ only in that region.

3) Slope Transfer Function $G_{\mathcal{X}\omega}(s)$: The transfer function from road slope to pedal cadence is a first-order low-pass filter, whose time constant T_ω has been derived in (14), with negative

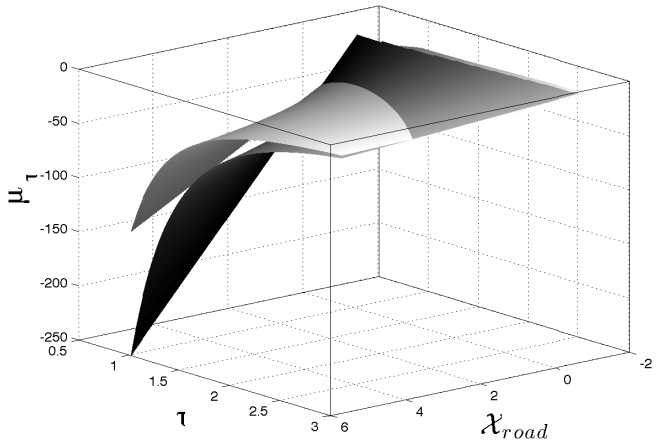

Fig. 6. Map of the gain μ_τ values with respect to the considered linearization point.

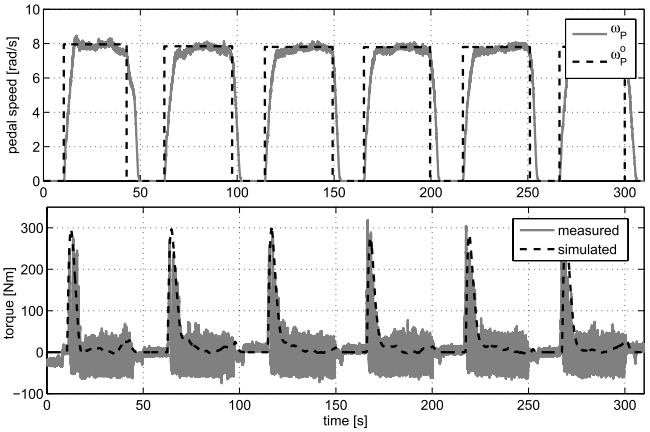

Fig. 7. Validation of the cyclist model.

gain

$$\mu_{\mathcal{X}} = -\frac{\overline{\tau}\Lambda\cos\left(\overline{\mathcal{X}}_{\text{road}}+\phi\right)}{D+2\sigma_2^*\overline{\tau}^3\overline{\omega}_p+\sigma_1^*\overline{\tau}^2} \tag{18}$$

indicating that the pedal speed decreases if the road slope increases. Although $\mu_{\mathcal{X}}$ depends on the equilibrium values of both road slope and transmission ratio, only the latter quantity has a measurable impact on the transfer function gain. The influence of $\overline{\mathcal{X}}_{\text{road}}$ is mitigated by the cosine function. On the other hand, the transmission ratio effectively acts as a scaling factor on the system gain, thus modulating the road slope effect on the speed ω_p.

The three inputs directly affect the pedaling power, which, as will be explained later, is the input of the HR model. The pedal power is defined as the product of the pedal speed and torque, $P = T_p\omega_p$. In an input/output perspective, the pedal power can be expressed as the sum of the three contributions

$$\delta P = G_T(s)\delta T_p + G_\tau(s)\delta\tau + G_{\mathcal{X}}(s)\delta\mathcal{X}_{\text{road}} \tag{19}$$

where the transfer function expressions can be easily obtained as

$$G_T(s)=\mu_1\frac{sT_1+1}{sT_\omega+1},\quad G_\tau(s)=\frac{\bar{T}_p\mu_\tau}{sT_\omega+1},\quad G_{\mathcal{X}}(s)=\frac{\bar{T}_p\mu_{\mathcal{X}}}{sT_\omega+1} \tag{20}$$

with $\mu_1 = \bar{\omega}_p + \bar{T}_p\mu_T$ and $T_1 = \bar{\omega}_p T_\omega/\mu_1$.

It is worth noticing that the structure of the transmission ratio and the slope transfer functions is exactly the same of the transfer functions $G_{\tau\omega(s)}$ and $G_{\xi\omega(s)}$ analyzed before, which link the two quantities to the pedal speed, from which they differ for the gain value only. On the contrary, one zero arises in the transfer function $G_T(s)$ that was not present in $G_{T\omega}(s)$. This correctly models the direct connection that exists between pedaling power and torque.

B. Cyclist

From the control point of view, the bicycle has three inputs: the controllable transmission ratio that is modeled by (4), the cyclist's torque and the road slope. The CVT ratio is the control input. The road slope is an unmeasurable (in this application, measuring the slope would require an inertial measurement unit [9]) disturbance; it is exogenous and not influenced by any other input. On the other hand, the cyclist's torque, which is also an unmeasurable disturbance, is correlated with the other inputs. In fact, the cyclist responds to variations in both transmission ratio and road slope. This causality relation needs to be accounted for and modeled.

To better understand this issue, consider the power linearized dynamics (19). It yields a negative gain between transmission ratio and pedaling power. This seems to contradict experimental results and common sense. The cyclist associates an increase of the transmission ratio to an increase in pedaling power. The reason for this apparent discrepancy is that the cyclist herself is a control system.

Evidence suggests [33] that during normal cycling, the cyclist acts as a pedaling cadence controller, imposing the pedal torque and comparing the desired pedal cadence with the current one. In order for the model to be complete and usable to design a HR controller, also this aspect must be considered.

To this end, a set of experiments was used to identify the linear pedal cadence controller that models the rider's behavior. In the experiments, performed with a constant transmission ratio, the rider was asked to accelerate to a constant velocity starting from standstill. The final steady state velocity is assumed to be the reference velocity. The model is identified minimizing the prediction error between the measured torque and the one computed when the model is fed with the same velocity tracking error. The resulting pedaling cadence controller has the following structure:

$$R_{H\omega}(s) = \mu_{H\omega}\frac{(1+sT_{zH\omega})}{(1+sT_{pH\omega})^2} \tag{21}$$

whose parameters are $\mu_{H\omega} = 60$, $T_{zH\omega} = 0.08$, and $T_{pH\omega} = 0.65$. Fig. 7 plots the validation of the identified model.

Note that the cyclist's model is needed to account for the effect of a variation in the transmission gear onto the pedaling power. The HR controller does not use any information on the current and desired velocity.

Considering the cyclist in the loop and computing the new transfer function from transmission gear to pedaling power, one obtains

$$G_{\tau P}(s) = \frac{G_\tau + R_{H\omega}(G_{T\omega}G_\tau - G_{\tau\omega}G_T)}{1 + R_{H\omega}G_{\tau\omega}}. \qquad (22)$$

The resulting transfer function model $G_{\tau P}(s)$ presents some interesting features.

1) The model gain is now positive, thus well explaining the real system behavior i.e., if the transmission ratio increases also the power increases, as the cyclist experiences.
2) The main time constant of (22) is noticeably faster than the one of the transfer function G_τ. This is due to the pedal cadence controller. Fig. 7 offers a qualitative explanation of this phenomenon: in the initial part of the experiment (i.e., during the departure), the torque peaks to high values before reaching steady state.
3) The transfer function (22) is nonminimum phase, as one of its zeros has a positive real part. The resulting inverse response can be intuitively explained as a residual effect of G_τ. As a matter of fact, if τ increases, the cyclist needs a small time interval to adapt the torque to this variation. During this phase, the pedal speed (and therefore the power) decreases, exhibiting the typical inverse behavior. The same holds for a change in τ in the opposite direction.

C. HR Dynamics

In Section I, it has been shown that a rich literature exists on the topic of HR dynamic modeling. Among the available models, the Hammerstein approach presented [31] is adopted herein. Hammerstein models have several advantages that make them desirable control-oriented models. The most important advantage is that they are capable of describing nonlinear dynamics, while retaining some linear properties. This allowed researchers to develop identification and control system design tools that are not available for other nonlinear models.

A Hammerstein model is constituted by the series connection of a static nonlinearity $\mathcal{N}$ and a linear dynamical system with state-space matrices A–D

$$\begin{aligned} \dot{x}(t) &= Ax(t) + B\tilde{u}(t) \\ z(t) &= Cx(t) + D\tilde{u}(t) \\ \mathrm{HR}(t) &= \mathrm{HR}_0 + \gamma\, z(t) \qquad \tilde{u}(t) = \mathcal{N}(u(t)) \end{aligned} \qquad (23)$$

where the model output $z(t)$ is a scaled version of the HR variations from the basal value, while $u(t)$ represents the input power. One of the advantages of using a Hammerstein model is that the static nonlinearity and linear dynamics can be decoupled [2].

In deriving a HR dynamic model, one has to face two challenges. First, subjects of different age, fitness, and health conditions respond differently to the same exercise. Second, even when considering a single subject, the HR dynamics are affected by numerous factors. Some of them are not controllable (e.g., temperature, humidity, and stress level); some of them are controllable. In the following, everything that is not controllable will be considered as uncertainty. The controllable factors are on the other hand studied in details. The CVT can influence pedal power, cadence, and torque. All of them are therefore potential candidate inputs. The following discussion starts from the simplifying assumption that HR mainly depends on the pedaling power to then validate it *a posteriori*.

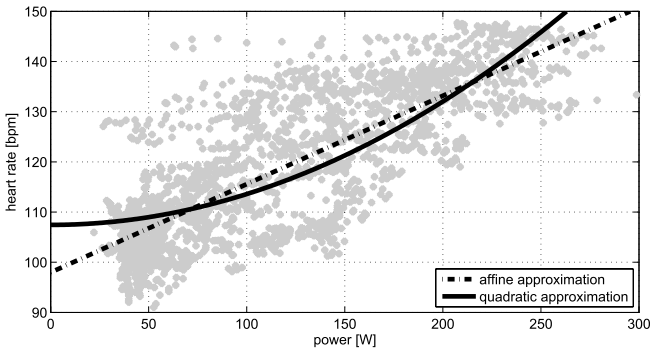

Fig. 8. Measured power/HR steady-state characteristic (dots), affine and quadratic approximations.

To study the HR dynamics, two sets of experiments were considered: first, a series of slowly varying power profiles was required to the cyclist, to assess the steady-state relationship between pedal power and HR, i.e., the model nonlinearity $\mathcal{N}$. Then, some dynamical experiments were carried out, so as to capture the main system dynamics. The envisioned field of application guides the experiment design: the experiments need to excite the HR dynamics in a realistic HR range for the application (Section IV).

For the first experiment, the cyclist was asked to keep a constant pedaling cadence, while the bicycle transmission ratio is varied so as to produce a sinusoidal power varying from 50 to 300 W. The resulting quasi-static input/output relation is shown in Fig. 8, where the cyclist's HR is plotted as a function of pedaling power.

To explain the relationship between the two quantities, two different models are proposed

$$\begin{aligned} \boldsymbol{\mathcal{N}}_{\mathrm{lin}} &: \hat{\mathrm{HR}} = a_1 + a_2 P \\ \boldsymbol{\mathcal{N}}_{\mathrm{par}} &: \hat{\mathrm{HR}} = a_3 + a_4 P^2. \end{aligned} \qquad (24)$$

The first model, $\boldsymbol{\mathcal{N}}_{\mathrm{lin}}$, forces an affine characteristics, while the quadratic model $\boldsymbol{\mathcal{N}}_{\mathrm{par}}$ follows from the hints of [21]. From Fig. 8, it can be observed that both models fit the data. The resulting coefficient of determinations is $R^2_{\mathrm{lin}} = 0.642$ and $R^2_{\mathrm{par}} = 0.584$; the use of a more complex quadratic curve is not justified by the added accuracy, so that the affine approximation is selected. The quadratic nonlinearity would be more adequate to model the HR dynamics in case of more intense exercise, as it can ensure a more accurate fitting of the measured HR (see [21] and references therein). The linear approximation, however, provides a good accuracy for the power levels usually involved in leisure and commuting cycling and can be sufficient for the purposes of this paper.

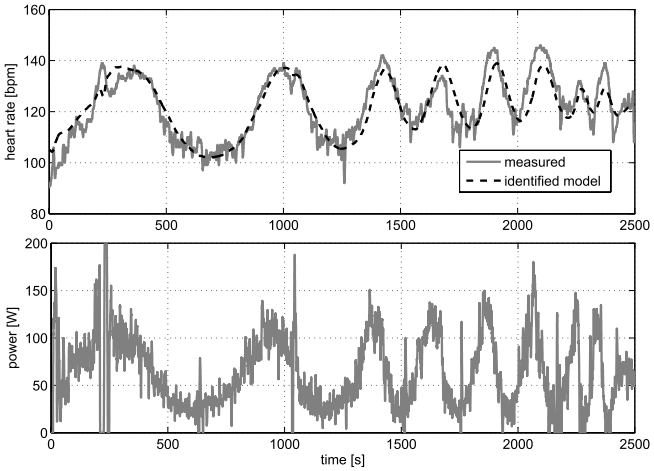

Fig. 9. Power sweep and corresponding HR (measured and simulated).

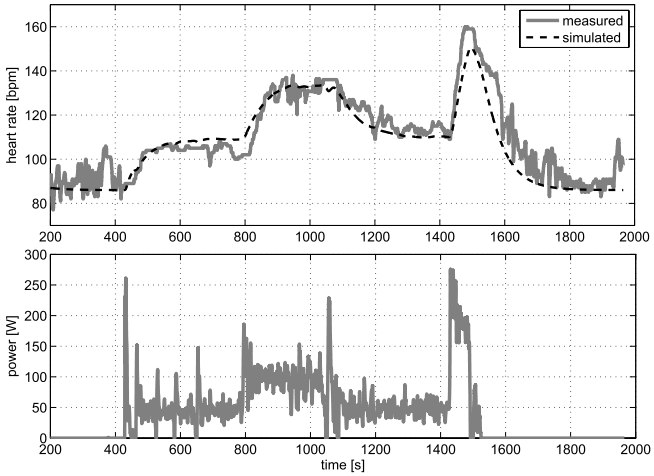

Fig. 10. HR model validation on subject 1. Measured and simulated HR and pedaling power.

In view of the results obtained for the identification of the static map, the system can be assumed to be linear and its dynamics identified by means of prediction error minimization identification methods for linear systems. A series of pedal power frequency sweeps is executed with the same methodology as before. The measured HR response in one of these experiments is shown in Fig. 9 together with the identified model output.

From the collected data, a nonparametric estimate of the system frequency response $G_{\mathrm{HR}}(j\omega)$ is obtained by windowed spectral analysis of the input/output cross-spectral densities [24]. The data are preprocessed by removing the basal HR (termed HR_0) and an additional linear trend. A second-order fitting of the experimental frequency response yields the parametric transfer function model

$$G_{\mathrm{HR},1}(s) = \frac{\mu_{\mathrm{hr}}}{(sT_{\mathrm{hr1}}+1)(sT_{\mathrm{hr2}}+1)} \tag{25}$$

with $T_{\mathrm{hr1}} = 22$ and $T_{\mathrm{hr2}} = 55$.

The linear trend represents the dynamics of the long-term fatigue [15]. This contribution is effectively modeled by an integral term $\mathrm{HR}_{\mathrm{FF}}$

$$G_{\mathrm{HR},2}(s) = \frac{\mu_{hF}}{s} u_2 \tag{26}$$

where the integrator gain $\mu_{hF} = 0.004$ was identified from the measured data and the binary control signal input signal u_2 simply indicates whether the cyclist is pedaling or not. The HR is constrained within $\mathrm{HR}_0 \leq \mathrm{HR}(t) \leq \mathrm{HR}_{\max}$; this is enforced with an antiwindup configuration. The HR of the considered subject is therefore given by

$$G_{\mathrm{HR}}(s) = G_{\mathrm{HR},1}(s) + G_{\mathrm{HR},2}(s). \tag{27}$$

For model validation, two different experiments were considered. The first validation test is performed on subject 1. Fig. 10 plots the time histories of the measured HR and the required power, together with the simulated HR model output.

The experiment yields a normalized root mean square (rms) simulation error of $\mathcal{J}_{\mathrm{rms}} = 8.2\%$, regarded as satisfactory for a control-oriented model.

As pointed out above, the proposed model (27) is power driven. It assumed that the cyclist's HR depends exclusively on the pedaling power. This is a simplifying assumption. Power is determined by pedaling torque and cadence, and they could influence the HR independently. Potentially, the model could have two degrees of freedom. To investigate the validity of this modeling choice for the considered application, the second subject performed two types of experiments.

1) *Iso-Speed Test*: In this test, the rider keeps the pedal speed as constant as possible, while the transmission ratio is varied by the ECU so as to produce a desired power profile.
2) *Iso-Torque Test*: In this test, the rider provides the same power levels reached in the previous tests, while keeping the pedal torque as constant as possible, therefore varying the pedal speed. As before, the transmission ratio was varied by the ECU so as to produce a desired power profile, while the rider, behaving now as torque regulator, varies the pedal speed to keep the torque to the desired level.

Fig. 11 plots the time histories of HR and power measured in these experiments, together with the simulated HR model outputs. The model output is very close to the measured HR with $\mathcal{J}_{\mathrm{rms}} = 6.12\%$ (iso-torque) and $\mathcal{J}_{\mathrm{rms}} = 6.05\%$ (iso-speed). These results support the choice of a power-driven HR dynamic model.

A control-oriented model of the entire system is now available. It captures the main dynamic features useful for control system design; it is not an attempt to exhaustively capture all dynamic aspects in all conditions. The model parameters have been identified and validated referring to a very specific usage i.e., leisure or commuting cycling for healthy persons. The proposed model will probably fail if tested under very different conditions (e.g., performance cycling).

As a matter of fact, a certain model variability is to be expected even in the considered conditions and possibly also with the same subject at different time of the day. In particular, a considerable variability of the steady-state characteristic has

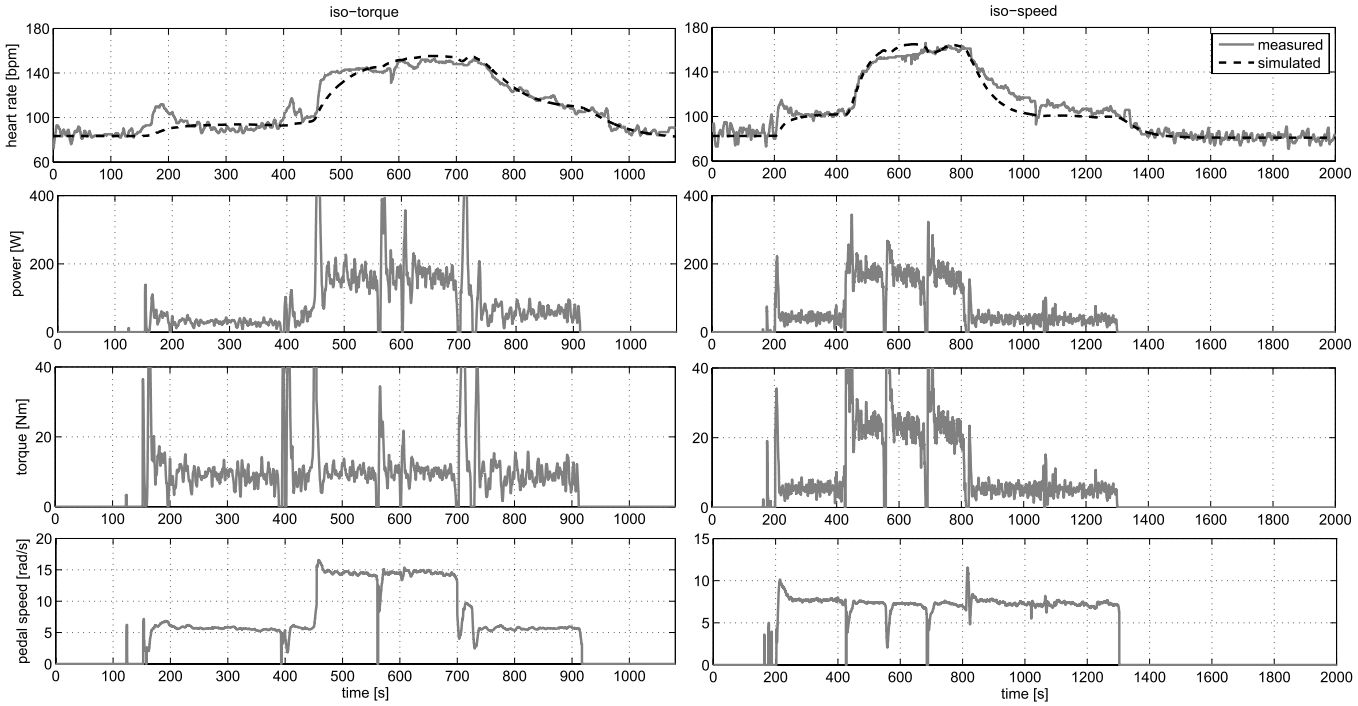

Fig. 11. HR model validation on subject 2. Iso-torque (left) and iso-speed (right) tests. Measured and simulated HR, pedaling power, torque, and cadence.

been recorded as a function of the overall fitness of the subject. These challenges are to be accounted for designing the controller.

III. Control System Design

The cyclist's HR control system should rely only on HR measurements and be robust to intersubject HR dynamic variability. In this section, two control approaches are investigated: a classical linear-loop shaping controller and a SOSM controller.

The linear controller design is carried out in two phases. First, a nominal controller has been designed based on the overall transmission ratio-to-HR transfer function

$$G(s) = G_{\tau P}(s) G_{\mathrm{HR}}(s) \tag{28}$$

linearized around nominal working conditions ($\tau = 1.5$ and $\omega_p = 90$ r/min), where $G_{\tau P}(s)$ is the dynamic description of the vehicle including the rider's pedal speed controller in (22) and $G_{\mathrm{HR}}(s)$ is the transfer function relating the cyclist's power to his/her HR. The design of the nominal controller is carried out using classical loop-shaping techniques with the objective of reaching a reasonable tradeoff between phase margin and bandwidth. Considerations on the uncertainties of the HR model lead to employ a controller with a proportional and integral action (implemented with an antiwindup scheme) with a nominal bandwidth of $f_c = 0.01$ Hz and a phase margin of $\varphi_m = 40°$. Subsequently, starting from the nominal controller, the parameters are fine-tuned via trial and error. Given the duration of the experiments needed to test the controller, this second phase is extremely time consuming.

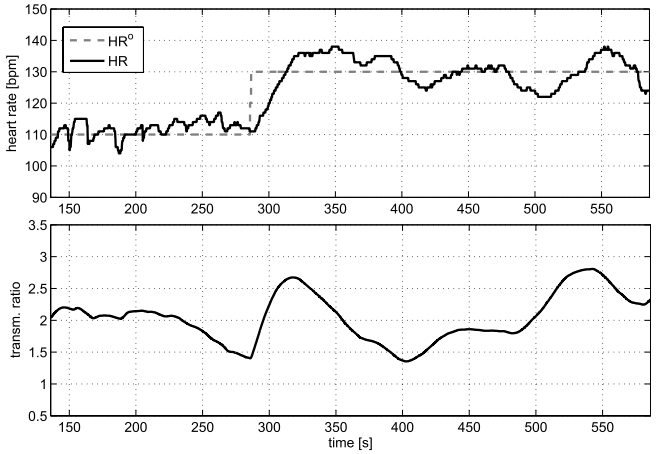

Fig. 12. Tracking performance of the PI controller.

HR set-point step variations while pedaling on a flat surface assess the performance of the controller. The results are shown in Fig. 12. The HR set point (HR°) has been varied from 110 to 130 bpm; these values require a moderate effort that the subject is capable of maintaining for prolonged periods of time. The following remarks are due.

1) The controller tracks the reference with a settling time of approximately 60 s.
2) As soon as the reference changes, the transmission ratio increases causing an increase in the pedaling power.
3) There are some tracking imperfections due to unmodeled HR dynamics, external disturbances (such as temporary and involuntary changes of speed and variations in the road surface and emotional-related HR changes).

The linear controller achieves a reasonable performance, but its fine-tuning is time consuming and there are no guarantees or robustness.

These limitations are overcome by the introduction of a SOSM controller of the suboptimal type [3], [34]. The choice of a SOSM controller over a first-order sliding mode one is dictated by the need of avoiding discontinuities in the control variable that would be perceived negatively by the cyclist. The controller is designed choosing the HR tracking error signal

$$e_{\mathrm{hr}}(t) = \mathrm{HR}^{\circ}(t) - \mathrm{HR}(t) \tag{29}$$

as the sliding variable. The control objective is to design a continuous control law τ° capable of steering this error to zero in finite time. Linearizing the complete model, the plant can be easily rewritten in the state-space form, as

$$\begin{aligned} \dot{z}(t) &= Az(t) + B\tau^{\circ}(t) \\ y(t) &= Cz(t) \end{aligned} \tag{30}$$

where $y(t)$ is the system output, i.e., the cyclist's HR, $z(t)$ is the system state vector, and the matrices A–C have appropriate dimensions. Based on this representation, the first- and the second-order time derivatives of the sliding variable e_{hr} are

$$\begin{cases} \dot{e}_{\mathrm{hr}} = \dot{y}^{\circ} + C\varrho \\ \ddot{e}_{\mathrm{hr}} = \varphi + \gamma\, \dot{\tau}^{\circ}(t) \end{cases} \tag{31}$$

where $\varrho = -Az - B\tau^{\circ}$, $\varphi = \ddot{y}^{\circ} + CA\varrho$, and $\gamma = -CB$. It can be shown [4], [23] that the control law

$$\begin{aligned} \dot{\tau}^{\circ}(t) &= -\eta(t) U \operatorname{sign}\ \left(e_{hr}(t) - \frac{1}{2} e_M \right) \\ \eta(t) &= \begin{array}{ll} \eta^* & \text{if } \left[e_{hr}(t) - \frac{e_M}{2} \right] e_M > 0 \\ 1 & \text{if } \left[e_{hr}(t) - \frac{e_M}{2} \right] e_M \leq 0 \end{array} \end{aligned} \tag{32}$$

where U is a control gain, η the modulation factor, and e_M a piecewise constant function taking the value of the last singular point of $e_{\mathrm{hr}}(t)$ (i.e., the most recent value e_M such that $\dot{e}_{\mathrm{hr}}(t_M) = 0$) drives the system trajectory to the sliding manifold $e_{\mathrm{hr}} = \dot{e}_{\mathrm{hr}} = 0$ in finite time if

$$\begin{aligned} \eta^* &\in (0, 1] \cup \left(0, \frac{3\Gamma_1}{\Gamma_2} \right) \\ U &> \max \left\{ \frac{\Phi}{\eta^* \Gamma_1}, \frac{4\Phi}{3\Gamma_1 - \eta^* \Gamma_2} \right\} \end{aligned} \tag{33}$$

where Γ_* and Φ are bounds of γ and φ such that

$$\begin{aligned} |\varphi| &\leq \Phi(z, y^{\circ}, \tau^{\circ}) \\ 0 &< \Gamma_1 \leq |\gamma| \leq \Gamma_2. \end{aligned} \tag{34}$$

In the considered application, the nominal value of the bounds on γ in (34) is $\Gamma_1 = \Gamma_2 = CB$; which is easily bounded considering all the possible operating conditions (linearization transmission ratio). The existence of $+\infty > \Phi \geq |\varphi|$ is guaranteed by the asymptotic stability of the system (30) and by the physical bounds on $\ddot{y}^{\circ}$ and τ°. Note that the control law is only based on the error measurement and does not require its time derivative.

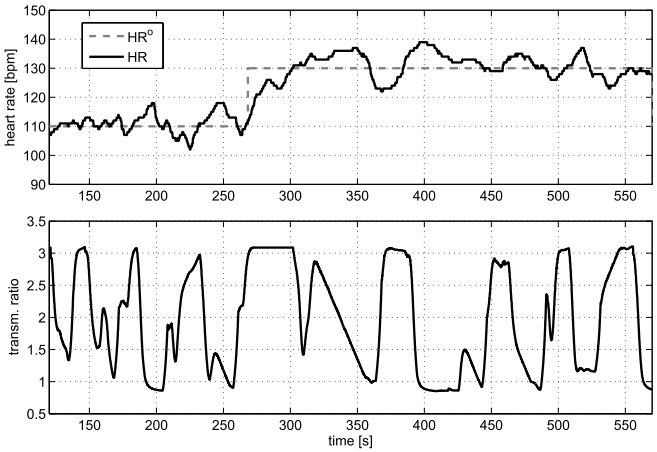

Fig. 13. Tracking performance of the SOSM controller.

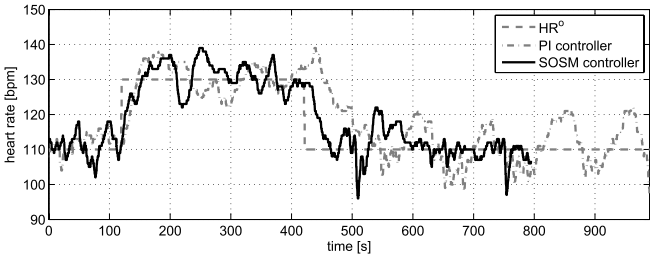

Fig. 14. Tracking performance comparison of the SOSM and PID controller.

Fig. 13 plots the results of a closed-loop HR step response, confirming that the SOSM controller is capable of ensuring the tracking of the desired HR with a continuous transmission ratio.

The comparison between the two controllers is better appreciated in Fig. 14. The figure plots a longer test with an ascending and descending step. In the ascending phase, the performance of the two controllers is similar in terms of reference tracking; note, however, the difference when the reference decreases to 110 bpm. The PI controller features some residual oscillations that were not present at the beginning of the exercise (when the reference was 110 bpm). These oscillations are attributed to the lack of robustness of the PI controller. The HR dynamics have changed between the initial and final phases of the exercise, and the robustness of the PI is challenged. Quantitatively, the tracking error rms of the PI controller is 7.5 bpm, whereas the SOSM controller yields an rms of 5.1 bpm. These step tests are useful to study the differences between the two controllers; however, to validate the overall system, more complete tests are needed. Considering the lack of robustness of the linear controller, along with the extremely time-consuming fine tuning phase, the SOSM controller represents a more interesting solution for further analysis.

IV. Validation

To further assess the effectiveness of the proposed approach, the SOSM controller was tested on a hilly urban test path.

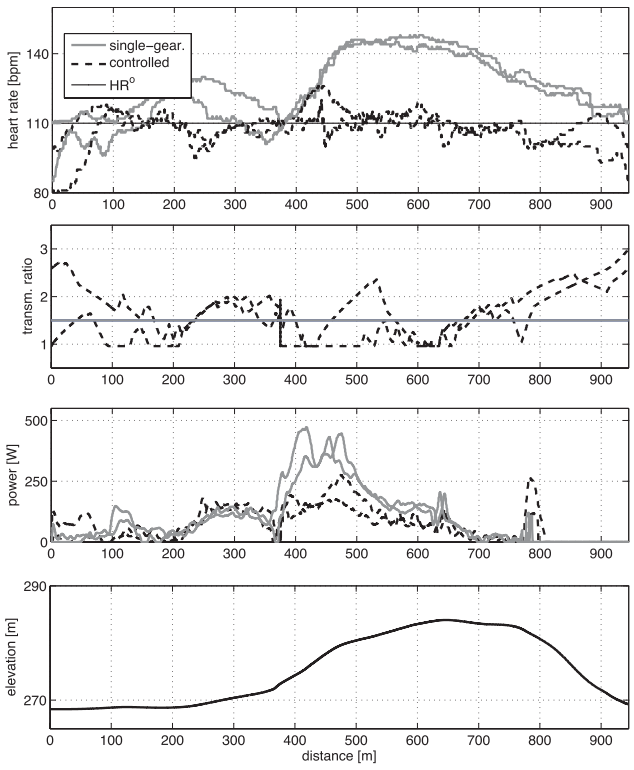

Fig. 15. HR controller validation on an urban path (subject 1).

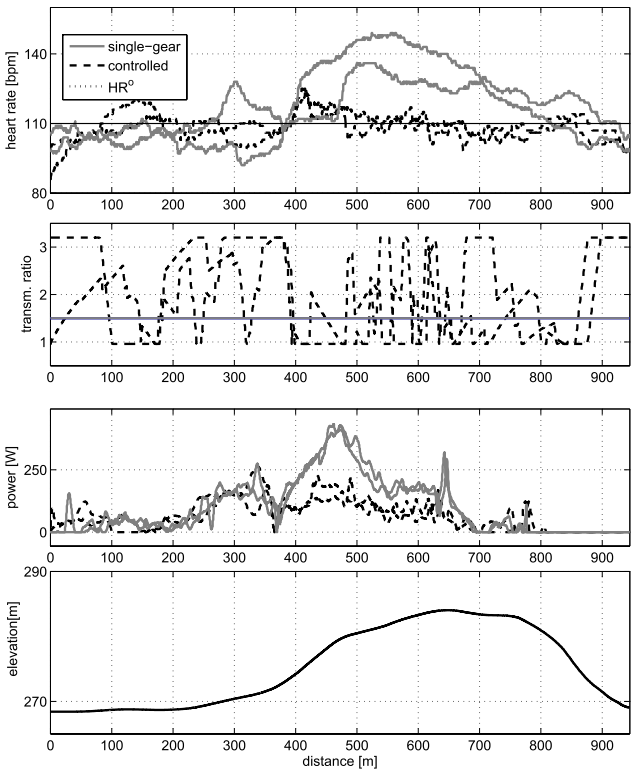

Fig. 16. HR controller validation on an urban path (subject 2).

Two additional healthy subjects (not involved in the modeling phase) were involved in the experiments. Both subjects have ridden the same bike in two configurations:

1) traditional single-gear mode (CVT set to $\tau = 1.5$);
2) HR controlled mode with a constant HR set point ($HR^\circ = 110$ bpm).

The urban path was ridden twice by each cyclist in each configuration. The cyclists were not given any specific instruction on how to ride the bicycle. Figs. 15 and 16 plot the results of these experiments, and Table I summarizes the quantitative results.

By inspecting the figures, some considerations are due.

1) In the single-gear case, the HR is strongly correlated with the road slope (see the bottom plot in the figure): when cycling at constant speed, slope is the main factor determining power variations.
2) The power profiles in the single-gear and controlled mode are similar until the uphill section. In this section, the controller effectively limits the cyclist's power.
3) The performance for subjects 1 and 2 is similar, showing that the proposed control is robust to variations in both cycling style and HR dynamic characteristics.
4) The controller successfully keeps the HR close to the desired set point HR° with small fluctuations.
5) The HR of the two cyclists in single-gear mode is rather different from one from the other. This is due to the riders' physical characteristics and their fitness level.
6) Unsurprisingly, the reductions in both HR variability and its average values come at a cost of a lower average speed for the trip.

TABLE I
QUANTITATIVE ANALYSIS OF THE VALIDATION RESULTS

	Subject 1		Subject 2	
	single-gear	CVT	single-gear	CVT
HR (BPM) (std.dev.)	124 (17.3)	111 (8.6)	117 (18)	109 (7)
mean velocity [km/h]	14.3	11.2	15.2	10. 6

V. CONCLUSION

In this paper, an integrated human-in-the-loop control of bicycle motion and HR regulation for noncompetitive cycling applications has been proposed. The controller, by adjusting the bicycle transmission ratio via a CVT, modulates the cyclist's effort to track a desired HR target. The design of the control system was guided by a thorough analysis of the system dynamics: control oriented models of the bicycle; cyclists and HR dynamics have been derived and validated using experimental data. The identified models suggest the use of robust control design techniques. Two approaches have been proposed a linear input–output controller tuned on the nominal model and a SOSM controller that is inherently more robust. The two controllers are validated using HR step responses on flat surfaces. Robustness considerations justify the choice of the SOSM controller for a more complete real-world usage validation, and two additional subjects were tested to show the effectiveness of SOSM controller in regulating the HR with low variability.

The use of a SOSM controller is one possible choice to account for the inevitable HR model uncertainties and variability. Another possible option could be that of using

the adaptive control framework, which is being considered for further development. Ongoing work is also being devoted to the online selection of the optimal HR reference, in the attempt of determining the best tradeoff between HR, fatigue, and overall cycling speed.

REFERENCES

[1] G. Alli, S. Formentin, and S. Savaresi, "On the suitability of EPACS in urban use," in *Proc. 5th IFAC Symp. Mechatron. Syst.*, 2010, pp. 277–284.

[2] E.-W. Bai, "Decoupling the linear and nonlinear parts in Hammerstein model identification," *Automatica*, vol. 40, no. 4, pp. 671–676, Apr. 2004.

[3] G. Bartolini, A. Ferrara, and E. Usani, "Chattering avoidance by second-order sliding mode control," *IEEE Trans. Autom. Control*, vol. 43, no. 2, pp. 241–246, Feb. 1998.

[4] G. Bartolini, A. Ferrara, A. Levant, and E. Usai, "On second order sliding mode controllers," in *Variable Structure Systems, Sliding Mode and Nonlinear Control*. New York, NY, USA: Springer-Verlag, 1999, pp. 329–350.

[5] S. E. Bearden and R. J. Moffatt, "Vo_2 and heart rate kinetics in cycling: Transitions from an elevated baseline," *J. Appl. Physiol.*, vol. 90, no. 6, pp. 2081–2087, 2001.

[6] E. Burke, *High-Tech Cycling*. Champaign, IL, USA: Human Kinetics, 2003.

[7] T. M. Cheng, A. V. Savkin, B. G. Celler, L. Wang, and S. W. Su, "A nonlinear dynamic model for heart rate response to treadmill walking exercise," in *Proc. 29th Annu. Int. Conf. IEEE Eng. Med. Biol. Soc. (EMBS)*, Aug. 2007, pp. 2988–2991.

[8] H.-C. Chien and C.-H. Tseng, "An automatic transmission for bicycles: A simulation," *Int. J. Ind. Ergonom.*, vol. 33, no. 2, pp. 123–132, Feb. 2004.

[9] M. Corno, P. Spagnol, and S. M. Savaresi, "Road slope estimation in bicycles without torque measurements," in *Proc. 19th IFAC Word Congr.*, Aug. 2014, pp. 6295–6300.

[10] R. Van der Plas, *Bicycle Technology: Understanding, Selecting and Maintaining the Modern Bicycle and Its Components*. Minneapolis, MN, USA: Motorbooks Int., 1991.

[11] Fallbrook Technologies Inc. (Jan. 2013). *Nuvinci Technology Website*. [Online]. Available: http://www.fallbrooktech.com

[12] P. Giani, M. Tanelli, and S. M. Savaresi, "Identification and control of a continuously variable transmission for bicycles," in *Proc. IET Conf. Control Autom., Uniting Problems Solutions*, Jun. 2013, pp. 1–6.

[13] P. Giani, "Modeling and control of automatic transmission systems in two-wheeled vehicles," Ph.D. dissertation, Dept. Elettron. Inf. Bioingegneria, Polytechnic Univ. Milan, Milano, Italy, 2014.

[14] P. Giani, M. Corno, M. Tanelli, and S. M. Savaresi, "Cyclist heart rate control via a continuously varying transmission," in *Proc. 19th IFAC World Congr.*, 2014, pp. 912–917.

[15] M. Hájek, J. Potůček, and V. Brodan, "Mathematical model of heart rate regulation during exercise," *Automatica*, vol. 16, no. 2, pp. 191–195, Mar. 1980.

[16] R. C. Hampshire and L. Marla, "An analysis of bike sharing usage: Explaining trip generation and attraction from observed demand," in *Proc. 91st Annu. Meeting Transp. Res. Board*, 2012, p. 17.

[17] R. Hess, J. K. Moore, and M. Hubbard, "Modeling the manually controlled bicycle," *IEEE Trans. Syst., Man, Cybern. A, Syst., Humans*, vol. 42, no. 3, pp. 545–557, May 2012.

[18] K. J. Hunt and D. B. Allan, "A stochastic Hammerstein model for control of oxygen uptake during robotics-assisted gait," *Int. J. Adapt. Control Signal Process.*, vol. 23, no. 5, pp. 472–484, May 2009.

[19] J. Lefever, D. Berckmans, and J.-M. Aerts, "Time-variant modelling of heart rate responses to exercise intensity during road cycling," *Eur. J. Sport Sci.*, vol. 14, pp. 1–7, Jul. 2012.

[20] J. P. Meijaard and A. L. Schwab, "Bicycle and motorcycle dynamics," *Veh. Syst. Dyn., Int. J. Veh. Mech. Mobility*, vol. 50, no. 8, p. 1191, 2012.

[21] S. Mohammad, T. M. Guerra, J.-M. Grobois, and B. Hecquet, "Heart rate control during cycling exercise using Takagi–Sugeno models," in *Proc. 18th IFAC World Congr.*, Milan, Italy, 2011, pp. 12783–12788.

[22] A. Muetze and Y. C. Tan, "Electric bicycles—A performance evaluation," *IEEE Ind. Appl. Mag.*, vol. 13, no. 4, pp. 12–21, Jul./Aug. 2007.

[23] W. Perruquetti and J.-P. Barbot, *Sliding Mode Control in Engineering*. Boca Raton, FL, USA: CRC Press, 2002.

[24] R. Pintelon and J. Schoukens, *System Identification: A Frequency Domain Approach*. New York, NY, USA: Wiley, 2001.

[25] T. Raviv, M. Tzur, and I. A. Forma, "Static repositioning in a bike-sharing system: Models and solution approaches," *EURO J. Transp. Logistics*, vol. 2, no. 3, pp. 187–229, 2013.

[26] A. L. Schwab and J. P. Meijaard, "A review on bicycle dynamics and rider control," *Veh. Syst. Dyn., Int. J. Veh. Mech. Mobility*, vol. 51, no. 7, pp. 1–32, 2013.

[27] S. C. Segerstrom and L. S. Nes, "Heart rate variability reflects self-regulatory strength, effort, and fatigue," *Psychol. Sci.*, vol. 18, no. 3, pp. 275–281, 2007.

[28] P. Spagnol *et al.*, "A full hybrid electric bike: How to increase human efficiency," in *Proc. Amer. Control Conf. (ACC)*, Jun. 2012, pp. 2761–2766.

[29] P. Spagnol, M. Corno, R. Mura, and S. M. Savaresi, "Self-sustaining strategy for a hybrid electric bike," in *Proc. Amer. Control Conf. (ACC)*, Jun. 2013, pp. 3479–3484.

[30] J. R. Stirling, M. Zakynthinaki, I. Refoyo, and J. Sampedro, "A model of heart rate kinetics in response to exercise," *J. Nonlinear Math. Phys.*, vol. 15, pp. 426–436, May 2008.

[31] S. W. Su, L. Wang, B. G. Celler, A. V. Savkin, and Y. Guo, "Identification and control for heart rate regulation during treadmill exercise," *IEEE Trans. Biomed. Eng.*, vol. 54, no. 7, pp. 1238–1246, Jul. 2007.

[32] S. W. Su *et al.*, "Nonparametric Hammerstein model based model predictive control for heart rate regulation," in *Proc. 29th Annu. Int. Conf. IEEE Conf. Eng. Med. Biol. Soc.*, Aug. 2007, pp. 2984–2987.

[33] P. Tandon, A. Awasthi, B. K. Mishra, P. Rathore, and R. K. Shukla, "Design and simulation of an intelligent bicycle transmission system," *IEEE/ASME Trans. Mechatronics*, vol. 16, no. 3, pp. 509–517, Jun. 2011.

[34] M. Tanelli, C. Vecchio, M. Corno, A. Ferrara, and S. M. Savaresi, "Traction control for ride-by-wire sport motorcycles: A second-order sliding mode approach," *IEEE Trans. Ind. Electron.*, vol. 56, no. 9, pp. 3347–3356, Sep. 2009.

[35] P. A. Watterson, "An electric assist bicycle drive with automatic continuously variable transmission," in *Proc. Int. Conf. Elect. Mach. Syst.*, Oct. 2008, pp. 2992–2997.

[36] M. S. Zakynthinaki and J. R. Stirling, "Stochastic optimization for modeling physiological time series: Application to the heart rate response to exercise," *Comput. Phys. Commun.*, vol. 176, no. 2, pp. 98–108, Jan. 2007.

[37] M. S. Zakynthinaki and J. R. Stirling, "Stochastic optimization for the calculation of the time dependency of the physiological demand during exercise and recovery," *Comput. Phys. Commun.*, vol. 179, no. 12, pp. 888–894, Dec. 2008.